optica

Self-starting bi-chromatic $LiNbO_3$ soliton microcomb

Yang He,[1,†] Qi-Fan Yang,[2,†] Jingwei Ling,[3] Rui Luo,[3] Hanxiao Liang,[1] Mingxiao Li,[1] Boqiang Shen,[2] Heming Wang,[2] Kerry Vahala,[2,4] and Qiang Lin[1,3,5]

[1]*Department of Electrical and Computer Engineering, University of Rochester, Rochester, New York 14627, USA*
[2]*T.J. Watson Laboratory of Applied Physics, California Institute of Technology, Pasadena, California 91125, USA*
[3]*Institute of Optics, University of Rochester, Rochester, New York 14627, USA*
[4]*e-mail: vahala@caltech.edu*
[5]*e-mail: qiang.lin@rochester.edu*

Received 3 June 2019; revised 29 July 2019; accepted 6 August 2019 (Doc. ID 369098); published 30 August 2019

The wide range of functions that are possible with lithium niobate (LN) waveguide devices, including phase and intensity modulation, second-harmonic generation, and difference-frequency generation, makes it attractive as a potential microcomb material. LN microcombs would combine essential comb self-referencing and control functions with the pulse generation process in a single microresonator device. Here, we demonstrate a soliton microcomb in a monolithic high-*Q* LN resonator. Direct frequency doubling of the soliton spectrum is observed inside the same cavity. The LN soliton mode-locking process also self-starts and allows bi-directional switching of soliton states, effects that are shown to result from the LN photorefractive effect. The Kerr solitons exhibit a self-frequency shift resulting from the Raman effect of LN. This microcomb platform can dramatically simplify miniature time keeping, frequency synthesis/division, and spectroscopy systems. Moreover, direct generation of femtosecond timescale pulses within LN microresonators can benefit quantum photonics and signal processing systems.

https://doi.org/10.1364/OPTICA.6.001138

1. INTRODUCTION

On-chip generation of optical frequency combs via Kerr nonlinearity has attracted significant interest in recent years [1], and the use of these devices for comb systems on a chip is being studied across a wide range of applications, including spectroscopy [2,3], communications [4], ranging [5,6], frequency synthesis [7], astrocombs [8,9], and optical clocks [10]. The recent realization of mode locking of Kerr microcombs [11], wherein the comb lines are mutually phase locked to form a stable soliton pulse train in time, is crucial for all of these applications. First observed in optical fiber systems [12], these coherently pumped solitons have now been demonstrated in microresonators made from silica [13,14], magnesium fluoride [11,15,16], silicon [17], and silicon nitride [16,18–21].

In this work, we report generation of Kerr solitons in high-*Q* lithium niobate (LN) resonators [22]. LN is of considerable interest for its versatile properties, including electro-optic as well as nonlinear optical effects [23–32]. The combination of these properties with stable soliton mode locking significantly amplifies the functionality of soliton microcombs and could potentially enable monolithically integrated comb systems as shown in Fig. 1(a). Moreover, another property of LN that has attracted somewhat less attention (the photorefractive effect [33,34]) is shown to provide important new soliton microcomb features including bi-directional switching control of multi-soliton states as well as self-starting. Finally, the Raman-induced self-frequency shift of soliton pulses is characterized.

2. MODE-LOCKED SOLITON STATES

To demonstrate both soliton generation as well as the self-starting feature, we employ a *z*-cut LN microresonator [Figs. 1(b) and 1(c)] with a loaded optical *Q* factor of 2.2×10^6 and a free-spectral range (FSR) of 199.7 GHz. Devices were dispersion engineered by control of a waveguide cross section to create anomalous group-velocity dispersion of $D_2/(2\pi) = 1.76$ MHz in the telecom band [Fig. 1(d)]. Details on the experimental setup as well as device characterization are provided in Supplement 1. Pump power of 33 mW is coupled onto the chip. The produced comb power [Figs. 1(e) and 1(f)] is monitored for pump frequency scanning in both tuning directions, which shows discrete steps, a signature of soliton mode locking. Single and multi-soliton states were readily observable—by stopping the laser at different steps. A single-soliton spectrum (mode spacing matches the resonator FSR), recorded at the first power step in Fig. 1(e), is shown in Fig. 1(g) and exhibits a smooth sech^2-shaped spectral envelope with a 3-dB bandwidth of ~27.9 nm. A two-soliton state spectrum is shown in Fig. 1(h), measured at the second power step in Fig. 1(e). It features a sinusoidal modulation with a period of 12 nm that is super-imposed on the sech^2-shaped spectral envelope.

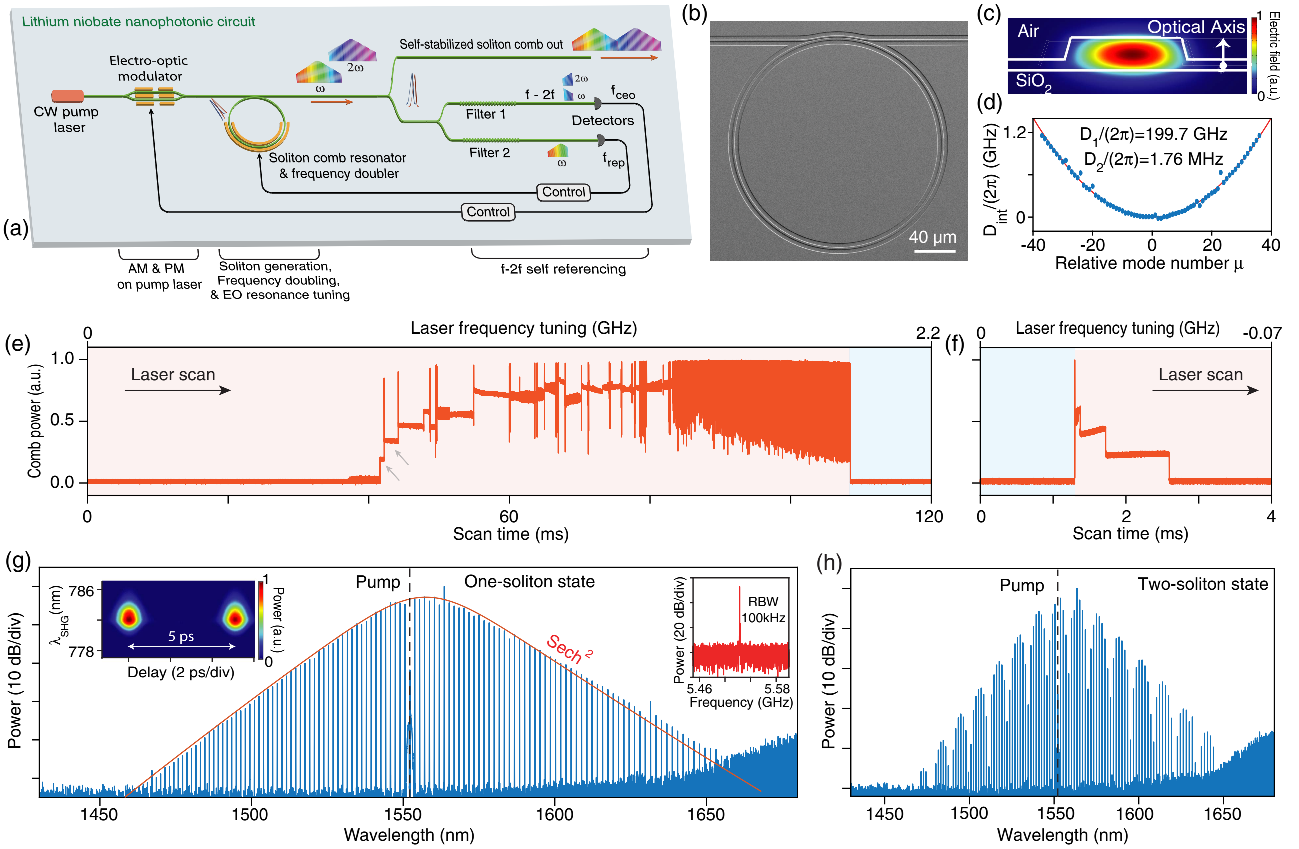

Fig. 1. Lithium niobate microresonator and mode-locked Kerr solitons. (a) Conceptual schematic of a lithium niobate nanophotonic circuit that enables all essential functions for a soliton comb system integrated on a single chip. These include soliton pulse generation, frequency doubling for self-referencing, and potential electro–optical control of the pump. (b) Scanning electron microscope image of a z-cut LN microring with a radius of 100 μm. (c) Schematic of the waveguide cross section of the microring. (d) Measured dispersion D_{int} plotted versus mode number for the soliton-forming mode family. See Supplement 1 for details. (e), (f) Comb power versus frequency tuning when the pump laser frequency is scanned from red to blue (e) and blue to red (f) across the pump resonance. The laser power is 33 mW on chip. The shaded red and blue regions correspond to approximate red-detuned and blue-detuned regions, respectively. (g), (h) Optical spectrum of the single-soliton (g) and two-soliton (h) state, respectively, measured at the first and second steps of the comb power in (e) (indicated by gray arrows). In (g), the red curve is a fitting to the theoretical sech^2 soliton spectral envelope. The left inset shows the corresponding FROG trace. The right inset shows the spectrum of a heterodyned beat note.

To further verify the single-soliton state at the first power step, we characterized the temporal waveform of the output pulses by frequency-resolved optical gating (FROG). As shown in the left inset of Fig. 1(g), the recorded FROG spectrogram gives pulse waveforms with a period of 5 ps, corresponding to the round-trip-time of the microresonator. To further characterize the coherence of the comb lines, a tunable external cavity diode laser was heterodyned with a microcomb line at ~1566.8 nm. The beat note exhibited a signal-to-noise ratio greater than 40 dB indicating the high coherence of the comb lines [right inset of Fig. 1(g)].

Accessing the soliton regime from the red detuning side as observed here has not been reported before and allows the soliton regime to be entered without the need for triggering techniques [1]. As we will show below, this is enabled by the photorefractive effect of LN, which allows the soliton mode locking to self-start. On the other hand, when the pump frequency is scanned from blue-detuned frequencies across the resonance, the step formation is not observed until the pump frequency enters into the red-detuned regime [Fig. 1(f)], at which point the power steps correspond to the first few steps in Fig. 1(e).

3. SECOND-HARMONIC GENERATION

LN exhibits a significant quadratic optical nonlinearity that can enable frequency up-conversion of the Kerr solitons inside the cavity, leading to a bi-chromatic soliton microcomb. This conversion is readily visible in the light scattered from the resonator as captured by a camera and spectrometer. As shown in Fig. 2(a), before the soliton microcomb is produced, the pump laser launched into the cavity generates only a small amount of second-harmonic (SH) scattered light. However, when the soliton is formed [Fig. 2(b)], its high peak power enhances the up-conversion process, resulting in a brighter image of the scattered SH light. Moreover, the SH spectrum exhibits an overall sech^2 shape. Figure 2(c) shows the SH signal produced from a soliton crystal [14] having a mode spacing of 6.4 nm (~800 GHz), four times that of the single-soliton state. The overall power of the soliton crystal is higher inside the cavity resulting in higher SH power generation and a considerably brighter image of the scattered light. The SH spectrum again exhibits a clear sech^2 shape. Frequency up-conversion of Kerr combs has been explored in various microresonators [35–37]. However, so far, up-conversion of Kerr solitons has not been demonstrated.

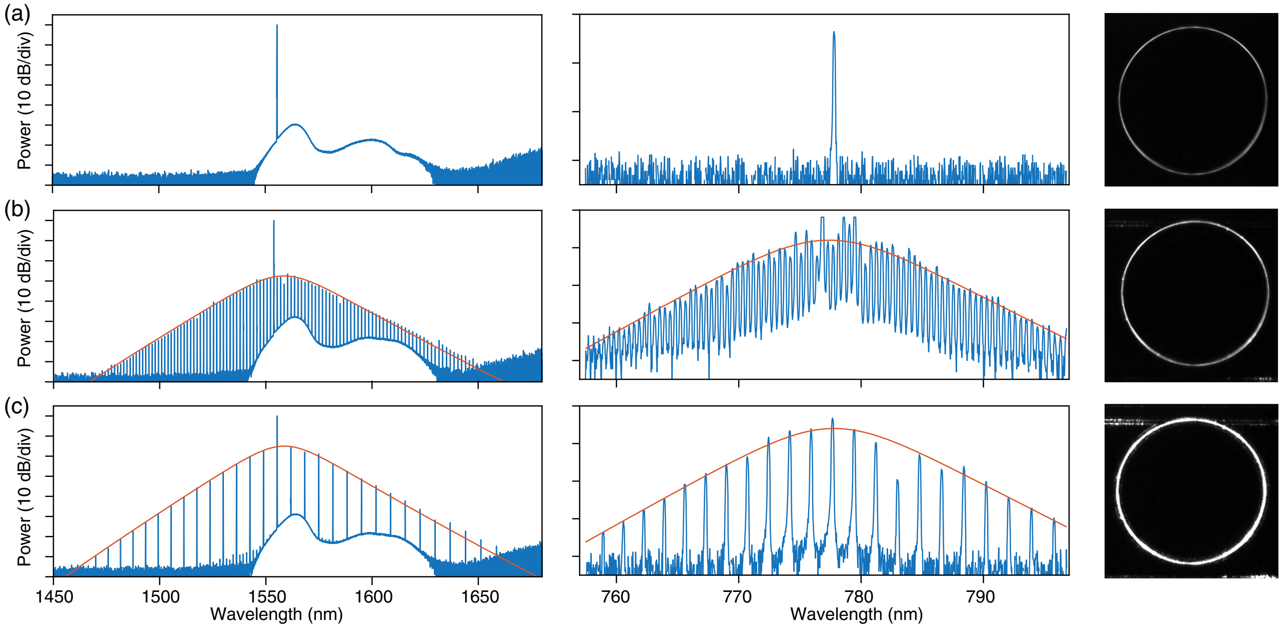

Fig. 2. Second-harmonic generation. (a) Optical spectra and device image before comb generation. (b) As in panel (a) but for a single-soliton state. (c) As in panel (a) but for a soliton crystal state. In all figures: left panel is the optical spectrum in the telecom band, recorded with a resolution of 0.05 nm; middle panel is the optical spectrum of generated second harmonic, recorded with a resolution of 0.15 nm; and right panel is the optical microscope image showing second-harmonic scattering from the resonator. The pump power is 23 mW on chip. In the produced second-harmonic combs (middle panels), the comb line spacing is ∼200 GHz and 800 GHz, respectively, for (b) and (c).

The bi-chromatic soliton microcombs observed here show that the LN soliton resonators have great potential for realizing direct on-chip f-to-2f signal generation, which is essential for comb self-referencing.

The coupling waveguide in the current device was designed for operation in the telecom band, and accordingly exhibits very low coupling efficiency for the SH signal. This also makes it challenging to identify the exact nature of the cavity modes associated with the produced SH combs. The SH coupling efficiency can be significantly improved with future optimization of the coupling-waveguide design [36].

4. SELF-STARTING AND BI-DIRECTIONAL SWITCHING OF SOLITON STATES

The processes for triggering the soliton mode-locked state and for switching between states having different soliton numbers are complicated by the presence of a well-known thermo-optic effect in high-Q resonators [38]. Accessing the soliton state has therefore prompted introduction of several techniques for power and frequency control so as to trigger and stabilize solitons [11,16,19,39]. Also, methods for deterministic control of soliton number through backward tuning have been developed as a direct result of the thermo-optic effect [16]. This form of tuning control is, however, unidirectional, meaning that the soliton number can be decreased only from an initial larger value that is itself determined by a stochastic process.

This situation is very different in the LN system. Here, the photorefractive effect causes an intensity-dependent decrease in refractive index [33,34] (opposite to that induced by the thermo-optic effect), and moreover the thermo-optic coefficient of the ordinary polarization in LN is relatively small around room temperature [40]. Therefore, if a microresonator is fabricated on a z-cut LN wafer, the quasi-transverse-electric (quasi-TE) cavity modes [Figs. 1(b) and 1(c)] will exhibit an optical bistability that stabilizes operation of the pump for red-detuned frequencies relative to the cavity resonance, as illustrated by the blue curve in Fig. 3(a). The inset of Fig. 3(a) shows a clear example. At the higher power level, the resonance features a triangular shape versus increasing pump frequency, opposite to that induced by thermo-optic nonlinearity [38]. As described in more detail below, this characteristic eliminates the well-known triggering problem in soliton microcombs, enabling soliton generation by tuning the pump directly into the red-detuned region [see Fig. 3(a)], i.e., without the need for any external triggering or high-speed frequency scanning mechanisms.

Of particular interest is that the stabilization introduced by the photorefractive effect enables bi-directional switching between different soliton states, a phenomenon that has so far been challenging in other soliton microcomb systems [1,41,42]. To demonstrate this phenomenon, the laser frequency was scanned up and down in frequency for red-detuned operation. As shown in Fig. 3(b), when the laser frequency increases, the comb power climbs up along discrete steps, indicating that the Kerr comb transits from a lower number to higher number of soliton states. Then, when the laser frequency decreases, the comb power steps down discretely, indicating a reverse transitioning of soliton states. Interestingly, an increase in soliton number is frequently accompanied by a power spike, while decreasing steps have no spiking behavior. Temporal resolution of the power spikes reveals a step-like substructure as shown in Fig. 3(c), I-IV. These spikes become less prominent when the laser scan speed is slowed as in Fig. 3(d).

The observed phenomena can be understood qualitatively by considering the schematic in Fig. 4. Kerr solitons exist within a

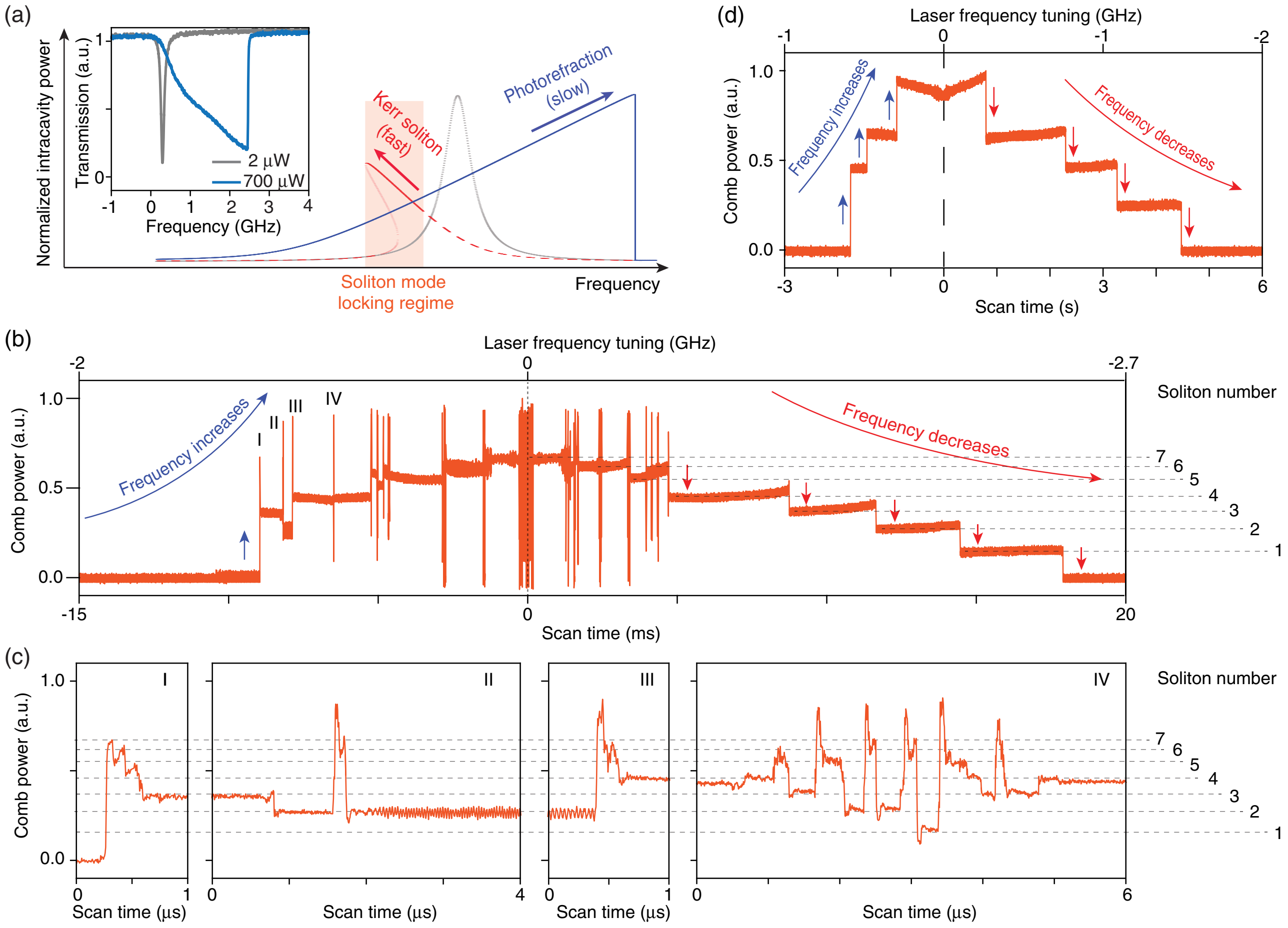

Fig. 3. Bi-directional switching of soliton states. (a) Schematic showing the resonance tuning induced by the optical Kerr effect, which shifts the resonance towards the red (red curve) on a short time scale, and the photorefractive effect, which shifts the resonance towards the blue (blue curve) on a much longer time scale. As a result, the stable soliton formation regime (shaded region) resides within the laser detuning regime that is stabilized by the photorefractive effect, thereby enabling self-starting soliton mode locking. The gray curve represents the intrinsic cavity resonance (with a certain photorefractive-induced tuning). The inset is measured power transmission versus pump frequency tuning (red to blue) for a quasi-TE cavity mode at two pump powers. The higher power behavior here results from the photorefractive effect and stabilizes the system for red-detuned operation. (b) Comb power measured as a function of time when the laser frequency is scanned forward and backward across a few soliton steps. The dashed lines give the number of solitons. (c) Temporally resolved waveforms of the power spikes indicated as I-IV in (b). The dashed lines indicate the number of solitons corresponding to those in (b). (d) Comb power measured as in (b) but using a slower laser frequency scanning speed.

specific red-detuning range of the pump frequencies relative to the cavity resonance [11,16]. When the pump laser is scanned towards the cavity resonance from the red-detuned side, it enters the existence range of a certain soliton state, ultimately exits near the resonance, and briefly enters a detuning regime where instabilities exist leading to the onset of the power spike (dark blue curve in Fig. 4). The photorefractive effect responds slowly (see Supplement 1) in comparison with the cavity lifetime. As a result, the accompanying increase in cavity power also causes a slower photorefractive tuning of the resonance to shorter wavelengths and away from the pumping frequency, thereby returning the system into the soliton existence detuning regime. Upon reentering the soliton existence regime, a soliton state is acquired with a certain number N of solitons, which occurs very quickly on a time scale set by the cavity lifetime. It is important to note that temporary passage into the unstable regime of pump detuning is critical for the soliton to form. Indeed, it allows the soliton states to self-start. With increased cavity power, the slower photorefractive effect continues blue shifting the cavity resonance further away from the pumping frequency. It causes the laser-cavity detuning to exit the soliton existence range, thereby forcing the system to acquire another soliton state. This process continues until the resulting detuning of the pump relative to the photorefractive-shifted cavity resonance is consistent with the soliton number that is inducing the photorefractive cavity shift.

The soliton dynamics described above are clearly visible in the transient power spiking process shown in Fig. 3(c), where the substructure can be readily associated with passage through the meta-stable soliton states described above, as the system ultimately achieves a self-consistent solution. The switching to a higher number of soliton states can become more regular and ordered if the laser scanning speed allows the photorefractive effect to stably settle, as shown in the case in Fig. 3(d). Finally, downward frequency tuning of the laser (red curve in Fig. 4) occurs in a similar manner. However, here, because the system is initially in a soliton state and because tuning occurs across the far edge of the soliton existence boundary (i.e., larger pump–cavity detuning), the system is never within the modulation

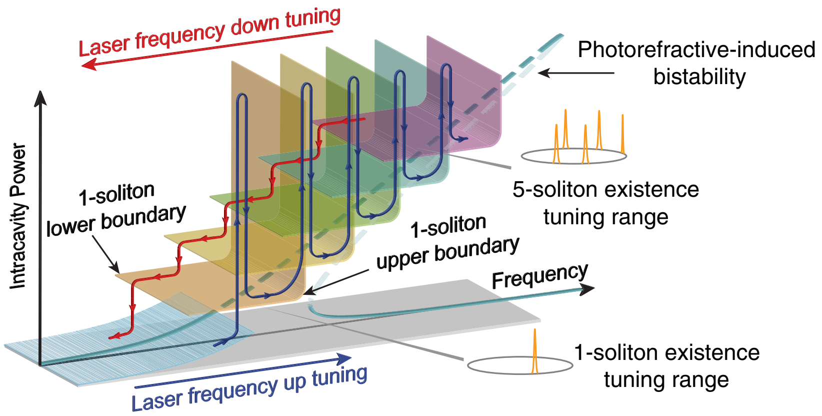

Fig. 4. Schematic showing the bi-directional switching of soliton states. Each L-shaped colored surface represents the existence frequency tuning range of a soliton state [11,16]. Different colors of L-shaped surfaces represent distinct soliton number states. The photorefractive effect adiabatically blue shifts the cavity resonance (dashed blue curve in the background) and thus disperses the existence tuning ranges of different soliton states over different frequency ranges. The dark blue curve gives the path of increasing soliton number states when the laser frequency is increased, while the red curve gives the path of decreasing soliton number states when the laser frequency is decreased.

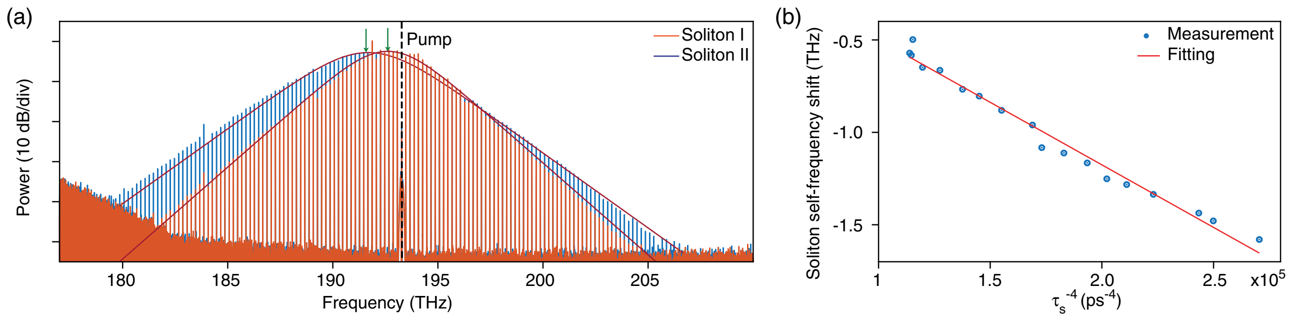

Fig. 5. Raman-induced soliton-self-frequency-shift. (a) Optical spectra for two single-soliton states with different spectral widths. The pump mode is indicated by the dashed black line, and the red curves are the fitted sech^2 envelopes, whose spectral centers are indicated by the green arrows. (b) SSFS as a function of $1/\tau_s^4$ with experimental points shown as blue dots and theoretical fitting [43] shown in red.

instability regime so that power spiking does not occur. A detailed study of these phenomena including numerical modeling is provided in Supplement 1.

5. SELF-FREQUENCY SHIFT OF KERR SOLITONS

The optical spectrum of the single-soliton state in Fig. 1(g) is not centered around the pump frequency, but rather is slightly shifted towards lower frequency. The effect is more evident in Fig. 5(a) where a larger spectral bandwidth results in a larger frequency shift. The frequency shift has been observed in silica and silicon nitride microresonators [13,43,44] and is related to the well-known soliton self-frequency shift (SSFS) induced by the intrapulse Raman scattering [45]. As shown in Fig. 5(b), the measured SSFS exhibits a linear dependence on $1/\tau_s^4$, where τ_s is soliton pulse width, consistent with the theory [43]. Fitting the measured linear dependence, we obtain the Raman shock time of congruent LN to be $\tau_R = 6.3$ fs. However, some differences in the nature of the Raman spectrum in LN versus other dielectrics require more study, and this fitting should be viewed as preliminary. Nonetheless, these results show the potentially crucial role of the Raman effect on ultashort pulse propagation in LN devices.

6. DISCUSSION

We have demonstrated a soliton microcomb in a LN microresonator. LN's photorefractive effect enables self-starting of soliton mode locking and bi-directional switching of soliton states, and its quadratic nonlinearity enables frequency doubling of the Kerr solitons and soliton crystals to produce bi-chromatic soliton microcombs. LN exhibits a variety of outstanding properties that are fairly unique among optical media [46]. For example, in addition to the Kerr, quadratic, and photorefractive optical nonlinearities that are utilized here, LN exhibits a strong electro-optic Pockels effect and a significant piezoelectric effect, which are ideal for high-speed spatiotemporal modulation and electro-mechanical tuning of nanophotonic circuits. Moreover, LN can be conveniently doped with rare-earth ions [47] to provide optical gain directly on chip. These important features would offer versatile approaches for controlling, manipulating, and modulating the soliton microcombs demonstrated here. Therefore, more generally, the demonstrations reported here open the door for realization of a multi-functional high-speed photonic signal processor for metrology, frequency synthesis/division, information coding, optical–optical/electro-optical waveband conversion, and other functions, all directly integrated on a single chip.

Note Added: During review of this paper, a report of soliton generation in LN was reported by [48]. We also call attention to our arXiv paper on LN solitons [22] cited in that report.

Funding. Defense Threat Reduction Agency (HDTRA11810047); National Science Foundation (ECCS-1810169, ECCS-1842691, EFMA-1641099, DMR-1719875); Air Force Office of Scientific Research (FA9550-18-1-0353).

Acknowledgment. This work was performed in part at the Cornell NanoScale Facility, a member of the National Nanotechnology Coordinated Infrastructure (National Science Foundation), and at the Cornell Center for Materials Research (National Science Foundation). The project or effort depicted was or is sponsored by the Department of the Defense, Defense Threat Reduction Agency. The content of the information does not necessarily reflect the position or the policy of the federal government, and no official endorsement should be inferred.

See Supplement 1 for supporting content.

[†]These authors contribute equally to this work.

REFERENCES

1. T. J. Kippenberg, A. L. Gaeta, M. Lipson, and M. L. Gorodetsky, "Dissipative Kerr solitons in optical microresonators," Science **361**, eaan8083 (2018).
2. M.-G. Suh, Q.-F. Yang, K. Y. Yang, X. Yi, and K. J. Vahala, "Microresonator soliton dual-comb spectroscopy," Science **354**, 600–603 (2016).
3. A. Dutt, C. Joshi, X. Ji, J. Cardenas, Y. Okawachi, K. Luke, A. L. Gaeta, and M. Lipson, "On-chip dual-comb source for spectroscopy," Sci. Adv. **4**, e1701858 (2018).
4. P. Marin-Palomo, J. N. Kemal, M. Karpov, A. Kordts, J. Pfeifle, M. H. P. Pfeiffer, P. Trocha, S. Wolf, V. Brasch, M. H. Anderson, R. Rosenberger, K. Vijayan, W. Freude, T. J. Kippenberg, and C. Koos, "Microresonator-based solitons for massively parallel coherent optical communications," Nature **546**, 274–279 (2017).
5. M.-G. Suh and K. J. Vahala, "Soliton microcomb range measurement," Science **359**, 884–887 (2018).
6. P. Trocha, M. Karpov, D. Ganin, M. H. P. Pfeiffer, A. Kordts, S. Wolf, J. Krockenberger, P. Marin-Palomo, C. Weimann, S. Randel, W. Freude, T. J. Kippenberg, and C. Koos, "Ultrafast optical ranging using microresonator soliton frequency combs," Science **359**, 887–891 (2018).
7. D. T. Spencer, T. Drake, T. C. Briles, J. Stone, L. C. Sinclair, C. Fredrick, Q. Li, D. Westly, B. R. Ilic, A. Bluestone, N. Volet, T. Komljenovic, L. Chang, S. H. Lee, D. Y. Oh, M.-G. Suh, K. Y. Yang, M. H. P. Pfeiffer, T. J. Kippenberg, E. Norberg, L. Theogarajan, K. Vahala, N. R. Newbury, K. Srinivasan, J. E. Bowers, S. A. Diddams, and S. B. Papp, "An optical-frequency synthesizer using integrated photonics," Nature **557**, 81–85 (2018).
8. E. Obrzud, M. Rainer, A. Harutyunyan, M. H. Anderson, J. Liu, M. Geiselmann, B. Chazelas, S. Kundermann, S. Lecomte, M. Cecconi, A. Ghedina, E. Molinari, F. Pepe, F. Wildi, F. Bouchy, T. J. Kippenberg, and T. Herr, "A microphotonic astrocomb," Nat. Photonics **13**, 31–35 (2019).
9. M.-G. Suh, X. Yi, Y.-H. Lai, S. Leifer, I. S. Grudinin, G. Vasisht, E. C. Martin, M. P. Fitzgerald, G. Doppmann, J. Wang, D. Mawet, S. B. Papp, S. A. Diddams, C. Beichman, and K. Vahala, "Searching for exoplanets using a microresonator astrocomb," Nat. Photonics **13**, 25–30 (2019).
10. Z. Newman, V. Maurice, T. E. Drake, J. R. Stone, T. C. Briles, D. T. Spencer, C. Fredrick, Q. Li, D. Westly, B. R. Ilic, B. Shen, M.-G. Suh, K. Y. Yang, C. Johnson, D. M. S. Johnson, L. Hollberg, K. Vahala, K. Srinivasan, S. A. Diddams, J. Kitching, S. B. Papp, and M. T. Hummon, "Photonic integration of an optical atomic clock," arXiv:1811.00616 (2018).
11. T. Herr, V. Brasch, J. D. Jost, C. Y. Wang, N. M. Kondratiev, M. L. Gorodetsky, and T. J. Kippenberg, "Temporal solitons in optical microresonators," Nat. Photonics **8**, 145–152 (2014).
12. F. Leo, S. Coen, P. Kockaert, S.-P. Gorza, P. Emplit, and M. Haelterman, "Temporal cavity solitons in one-dimensional Kerr media as bits in an all-optical buffer," Nat. Photonics **4**, 471–476 (2010).
13. X. Yi, Q.-F. Yang, K. Y. Yang, M.-G. Suh, and K. Vahala, "Soliton frequency comb at microwave rates in a high-Q silica microresonator," Optica **2**, 1078–1085 (2015).
14. D. C. Cole, E. S. Lamb, P. Del'Haye, S. A. Diddams, and S. B. Papp, "Soliton crystals in Kerr resonators," Nat. Photonics **11**, 671–676 (2017).
15. W. Liang, D. Eliyahu, V. S. Ilchenko, A. A. Savchenkov, A. B. Matsko, D. Seidel, and L. Maleki, "High spectral purity Kerr frequency comb radio frequency photonic oscillator," Nat. Commun. **6**, 7957 (2015).
16. H. Guo, M. Karpov, E. Lucas, A. Kordts, M. H. P. Pfeiffer, V. Brasch, G. Lihachev, V. E. Lobanov, M. L. Gorodetsky, and T. J. Kippenberg, "Universal dynamics and deterministic switching of dissipative Kerr solitons in optical microresonators," Nat. Phys. **13**, 94–102 (2017).
17. M. Yu, Y. Okawachi, A. G. Griffith, M. Lipson, and A. L. Gaeta, "Mode-locked mid-infrared frequency combs in a silicon microresonator," Optica **3**, 854–860 (2016).
18. V. Brasch, M. Geiselmann, T. Herr, G. Lihachev, M. H. P. Pfeiffer, M. L. Gorodetsky, and T. J. Kippenberg, "Photonic chip-based optical frequency comb using soliton Cherenkov radiation," Science **351**, 357–360 (2016).
19. C. Joshi, J. K. Jang, K. Luke, X. Ji, S. A. Miller, A. Klenner, Y. Okawachi, M. Lipson, and A. L. Gaeta, "Thermally controlled comb generation and soliton modelocking in microresonators," Opt. Lett. **41**, 2565–2568 (2016).
20. P.-H. Wang, J. A. Jaramillo-Villegas, Y. Xuan, X. Xue, C. Bao, D. E. Leaird, M. Qi, and A. M. Weiner, "Intracavity characterization of micro-comb generation in the single-soliton regime," Opt. Express **24**, 10890–10897 (2016).
21. Q. Li, T. C. Briles, D. A. Westly, T. E. Drake, J. R. Stone, B. R. Ilic, S. A. Diddams, S. B. Papp, and K. Srinivasan, "Stably accessing octave-spanning microresonator frequency combs in the soliton regime," Optica **4**, 193–203 (2017).
22. Y. He, Q.-F. Yang, J. Ling, R. Luo, H. Liang, M. Li, B. Shen, H. Wang, K. Vahala, and Q. Lin, "A self-starting bi-chromatic LiNbO3 soliton microcomb," arXiv:1812.09610 (2018).
23. L. Chen, Q. Xu, M. G. Wood, and R. M. Reano, "Hybrid silicon and lithium niobate electro-optical ring modulator," Optica **1**, 112–118 (2014).
24. J. Chiles and S. Fathpour, "Mid-infrared integrated waveguide modulators based on silicon-on-lithium-niobate photonics," Optica **1**, 350–355 (2014).
25. C. Wang, M. J. Burek, Z. Lin, H. A. Atikian, V. Venkataraman, I.-C. Huang, P. Stark, and M. Lončar, "Integrated high quality factor lithium niobate microdisk resonators," Opt. Express **22**, 30924–30933 (2014).
26. L. Chang, Y. Li, N. Volet, L. Wang, J. Peters, and J. E. Bowers, "Thin film wavelength converters for photonic integrated circuits," Optica **3**, 531–535 (2016).
27. R. Luo, H. Jiang, S. Rogers, H. Liang, Y. He, and Q. Lin, "On-chip second-harmonic generation and broadband parametric down-conversion in a lithium niobate microresonator," Opt. Express **25**, 24531–24539 (2017).
28. H. Liang, R. Luo, Y. He, H. Jiang, and Q. Lin, "High-quality lithium niobate photonic crystal nanocavities," Optica **4**, 1251–1258 (2017).
29. R. Wolf, I. Breunig, H. Zappe, and K. Buse, "Cascaded second-order optical nonlinearities in on-chip micro rings," Opt. Express **25**, 29927–29933 (2017).
30. C. Wang, M. Zhang, B. Stern, M. Lipson, and M. Lončar, "Nanophotonic lithium niobate electro-optic modulators," Opt. Express **26**, 1547–1555 (2018).
31. P. O. Weigel, J. Zhao, K. Fang, H. Al-Rubaye, D. Trotter, D. Hood, J. Mudrick, C. Dallo, A. T. Pomerene, A. L. Starbuck, C. T. DeRose, A. L. Lentine, G. Rebeiz, and S. Mookherjea, "Bonded thin film lithium niobate modulator on a silicon photonics platform exceeding 100 GHz 3-dB electrical modulation bandwidth," Opt. Express **26**, 23728–23739 (2018).
32. C. Wang, M. Zhang, R. Zhu, H. Hu, and M. Lončar, "Monolithic photonic circuits for Kerr frequency comb generation, filtering and modulation," Nat. Commun. **10**, 978 (2019).

33. P. Günter, J.-P. Huignard, and A. M. Glass, *Photorefractive Materials and Their Applications* (Springer, 1988), Vols. **1** and 2.
34. L. Maleki and A. Matsko, *Ferroelectric Crystals for Photonic Applications* (Springer, 2014), pp. 337–383.
35. S. Miller, K. Luke, Y. Okawachi, J. Cardenas, A. L. Gaeta, and M. Lipson, "On-chip frequency comb generation at visible wavelengths via simultaneous second- and third-order optical nonlinearities," Opt. Express **22**, 26517–26525 (2014).
36. X. Guo, C.-L. Zou, H. Jung, Z. Gong, A. Bruch, L. Jiang, and H. X. Tang, "Efficient generation of a near-visible frequency comb via Cherenkov-like radiation from a Kerr microcomb," Phys. Rev. Appl. **10**, 014012 (2018).
37. D. J. Wilson, K. Schneider, S. Hönl, M. Anderson, T. J. Kippenberg, and P. Seidler, "Integrated gallium phosphide nonlinear photonics," arXiv:1808.03554 (2018).
38. T. Carmon, L. Yang, and K. J. Vahala, "Dynamical thermal behavior and thermal self-stability of microcavities," Opt. Express **12**, 4742–4750 (2004).
39. X. Yi, Q.-F. Yang, K. Y. Yang, and K. Vahala, "Active capture and stabilization of temporal solitons in microresonators," Opt. Lett. **41**, 2037–2040 (2016).
40. L. Moretti, M. Iodice, F. G. D. Corte, and I. Rendina, "Temperature dependence of the thermo-optic coefficient of lithium niobate, from 300 to 515 K in the visible and infrared regions," J. Appl. Phys. **98**, 036101 (2005).
41. S. Zhang, J. M. Silver, L. Del Bino, F. Copie, M. T. M. Woodley, G. N. Ghalanos, A. Ø. Svela, N. Moroney, and P. Del'Haye, "Sub-milliwatt-level microresonator solitons with extended access range using an auxiliary laser," Optica **6**, 206–212 (2019).
42. Z. Lu, W. Wang, W. Zhang, S. T. Chu, B. E. Little, M. Liu, L. Wang, C.-L. Zou, C.-H. Dong, B. Zhao, and W. Zhao, "Deterministic generation and switching of dissipative Kerr soliton in a thermally controlled micro-resonator," AIP Adv. **9**, 025314 (2019).
43. X. Yi, Q.-F. Yang, K. Y. Yang, and K. Vahala, "Theory and measurement of the soliton self-frequency shift and efficiency in optical microcavities," Opt. Lett. **41**, 3419–3422 (2016).
44. M. Karpov, H. Guo, A. Kordts, V. Brasch, M. H. P. Pfeiffer, M. Zervas, M. Geiselmann, and T. J. Kippenberg, "Raman self-frequency shift of dissipative Kerr solitons in an optical microresonator," Phys. Rev. Lett. **116**, 103902 (2016).
45. J. P. Gordon, "Theory of the soliton self-frequency shift," Opt. Lett. **11**, 662–664 (1986).
46. R. Weis and T. Gaylord, "Lithium niobate: summary of physical properties and crystal structure," Appl. Phys. A **37**, 191–203 (1985).
47. W. Sohler, B. K. Das, D. Dey, S. Reza, H. Suche, and R. Ricken, "Erbium-doped lithium niobate waveguide lasers," IEICE Trans. Electron. **E88-C**, 990–997 (2005).
48. Z. Gong, X. Liu, Y. Xu, M. Xu, J. B. Surya, J. Lu, A. Bruch, C. Zou, and H. X. Tang, "Soliton microcomb generation at 2 μm in z-cut lithium niobate microring resonators," Opt. Lett. **44**, 3182–3185 (2019).